FRACTAL 3D MODELING OF ASTEROIDS USING WAVELETS ON ARBITRARY MESHES

André Jalobeanu
Automated Learning Group, USRA/RIACS
NASA Ames Research Center MS 269-4, Moffett Field CA 94035-1000, USA
ajalobea@email.arc.nasa.gov

Abstract: *In this work, we study the 3D geometry of the small bodies in our Solar System in order to derive a probabilistic model of such objects. Images taken by various spacecrafts seem to exhibit a fractal behaviour, which we propose to investigate by using a multiscale approach. The idea is to look for a scale-invariant model that could simply describe the statistics of the asteroid surfaces. In order to access the different scales, we need either a Fourier or a Wavelet transform that could be applied to the triangular mesh defining the object to analyze. Since the former transform could not be easily constructed on meshes (because of their irregularity), we use a wavelet transform instead. This analysis tool is designed to capture both scaling and spatial information on the object. The main novelty w.r.t. existing wavelet transforms on meshes consists of providing a local estimate of the scale. This way, we show that the suspected fractal properties are actually an efficient modeling tool, and we build a statistical model of asteroids. A possible application of this model is the dense 3D reconstruction from multiple images, which is an ill-posed inverse problem. Using the fractal approach as a prior model within a Bayesian framework should enable us to get an accurate estimate of the asteroid shape.*

Keywords: *Statistical modeling, Fractal surfaces, Wavelets, Subdivision Meshes, 3D Reconstruction*

1 INTRODUCTION: FRACTAL SURFACES IN NATURE

Fractals have long been used to synthesize realistic looking landscapes on Earth or other planets, because of their resemblance to natural objects [6]. From a qualitative point of view, they certainly exhibit similar properties, such as self-similarity. In this paper, we focus more on the quantitative description of landscapes in terms of mathematical models, than on the generation of natural-like surfaces. Furthermore, we are interested in modeling asteroids and small bodies which are closed surfaces, topologically different from flat open landscapes commonly used in surface simulation and modeling.

1.1 Fractal appearence of asteroids

There is no doubt asteroid-like objects show details at all scales (e.g. 433 Eros on Fig. 1). They also appear to be very similar in shape to natural relief found on Earth, which is known to have fractal properties. This motivates a more precise study of these objects, to check the mathematical fractal properties they seem to exhibit.

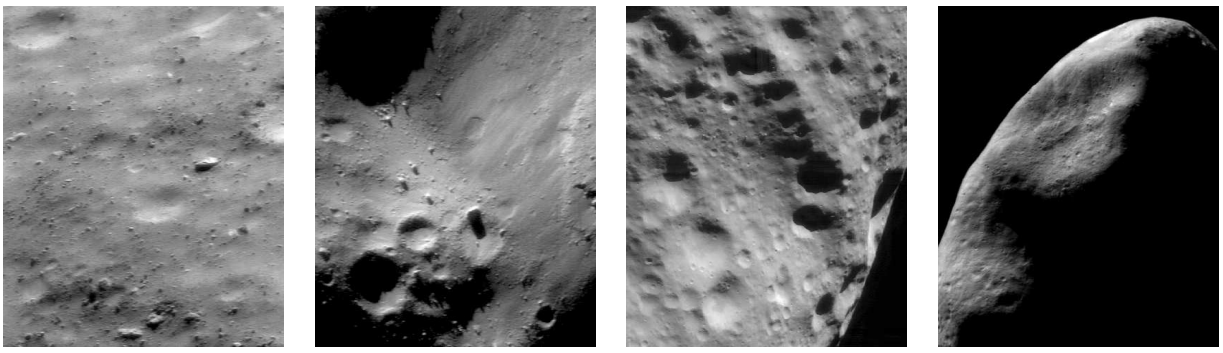

8 km 15 km 100 km 200 km

Figure 1: Images of the asteroid 433 Eros taken by the NEAR spacecraft from different distances, showing details at various resolutions illustrating the fractal behaviour of the surface (JPL/NASA).

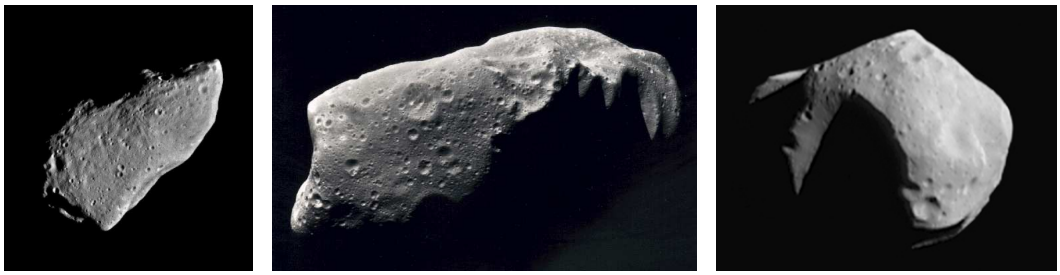

Figure 2: From left to right: asteroids Gaspra, Ida and Mathilde (JPL/NASA)

1.2 Studying fractal objects: what tool to use?

A possible way of studying fractals is to look for self-similarities. Statistical self-similarity is probably the easiest to check since we can use simple estimators instead of looking for repetition and scaling of particular geometrical shapes. If we find a scale invariant probability function fitting to the data, the object is said to be statistically scale invariant, and we can call it fractal. Let us consider the variation of the average size of object features as a function of the scale, regardless of the location. This is usually done using the power spectrum of the object, if it is available.

Planetary landscapes are quasi-planar surfaces (large enough w.r.t. the mountains, and small enough to consider that the planet is locally flat), therefore they can be efficiently modeled by a height field $h = f(x, y)$. Thus, the height can be encoded in a 2D image, and their study is facilitated by existing 2D tools such as the fast Fourier transform. However, asteroids have a rather different topology and, unless we only consider a small part of them, they need a different support to be properly described.

On Fig. 2 several bodies are shown; all of them have the same topology as a sphere (i.e. they are closed surfaces without holes). The sphere is still only a topological description, since the objects' geometry is far more complex. The spherical coordinates (r, φ, θ) are commonly used to describe planetary geometry using a spherical height field $r = F(\varphi, \theta)$. However it is not the best way of dealing with such surfaces because the sampling is highly irregular for two reasons: the radius variations are large w.r.t. the object radius, and the regular sampling of the longitude and latitude lead to an irregular grid. Thus, we prefer not to use the most standard approach in spherical spectrum analysis which involves spherical harmonics. But we still need to access the scale of the geometric features, which requires a more regular sampling of the surface.

2 WAVELETS ON MESHES WITH AN ARBITRARY TOPOLOGY

2.1 Topology and geometry

Before introducing the new tools used for surface analysis, we want to insist on two definitions involving the concept of regularity. First, regarding the topology: the topological support is the set of sites on which one can define a data sample, such as a 3D point in space. This support is regular if all the sites have the same neighborhood structure (for instance the same number of neighbors). We also refer to this property by topological sampling uniformity.

Once the topological space has been sampled by creating a set of sites and neighborhood systems, the geometry is defined on this support by associating a 3D point with each site. Thus, the geometric sampling of the surface can be irregular even though the topological support is regular. However, the regularity of the support is of prime importance in defining the wavelet transform in the following sections.

The mesh, or surface model, is defined by the set of vertices.

2.2 Subdivision meshes and vertex prediction

Triangular meshes provide a support which, if constructed carefully, can cover spherical surfaces regularly enough. If we consider an icosahedron (12 vertices defining 20 equilateral triangles), each vertex has 5 neighbors, and provides a topologically regular sampling of the sphere. But such a simple object can hardly be used because of the small number of samples. A nice way of taking advantage of the regularity and adding more points to a sphere is to construct a subdivided mesh [8, 7], starting for instance from an icosahedron, and recursively adding a vertex between each pair of existing vertices (see Fig. 3). Thus we define the topological subdivision, leading to a semi-regular mesh: each vertex has either 5 or 6 neighbors (only the 12 initial vertices have 5 neighbors, the others have 6). The subdivision is performed recursively up to level $J > 0$.

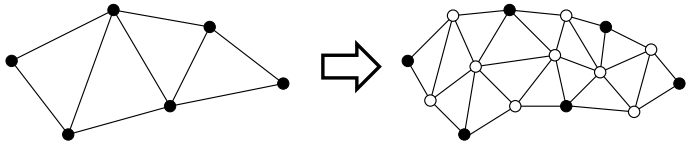

Figure 3: Subdivision scheme used to produce a finer mesh from an existing triangular mesh: a new vertex (white) is added between each pair of 2 vertices (black), using a prediction or interpolation rule.

Any asteroid can now be virtually represented using this support. To perform real data analysis we first need to associate a 3D point to each topological site. Since available 3D models are provided as spherical height fields, we create a unit sphere and then replace each point radius by $H(\varphi, \theta)$.

Regarding the geometry, the key point of this subdivision scheme is the new vertex prediction. This prediction is achieved by interpolation. The simplest scheme consists of assuming piecewise linearity and taking the middle point of the edge, but leads to an unwanted piecewise planar surface (we keep the initial icosahedron shape). Therefore we prefer using a smooth subdivision called Butterfly scheme [2], involving 8 parents for each new vertex (see Fig. 4 a). In the regular case when both edge vertices have 6 neighbors, the new vertex m is given by:

$$m = B(\{v\}) \equiv \frac{1}{2}\left(v_1^1 + v_2^1\right) + \frac{1}{8}\left(v_1^2 + v_2^2\right) - \frac{1}{16}\left(v_1^3 + v_2^3 + v_3^3 + v_4^3\right) \tag{1}$$

where the upper and lower indices respectively denote the neighborhood order and a spatial index. In the other cases we use a modified scheme [12] where the coefficients in Eq. (1) depend on the valence of the vertices.

2.3 Construction of a lifted wavelet transform

The prediction function B is used to construct a wavelet transform on the sphere [8], using the lifting scheme [10].

A subdivided mesh at level J is given. The basic idea is to split the sites into two interleaved sets: the midpoints $\{m\}$ and the closest parents $\{v^1\}$ (respectively white and black points on Fig. 3). Then, the former are predicted from the latter using the function B. The difference between actual and predicted vertices gives us the wavelet details, and is located at the same sites as $\{m\}$:

$$w = m - B(\{v\}) \tag{2}$$

These coefficients encode the details at a given level, since they represent the difference between a smooth approximation of the surface and the actual surface.

The non-lifted wavelet transform consists of recursively applying this algorithm to the set of remaining vertices $\{v^1\}$. At each level, this set is called the wavelet approximation a and is obtained by simple decimation, or inverse step of the subdivision. The wavelet functions corresponding to this transform still do not have sufficient smoothness properties, related for instance to spectral selectivity, needed to analyze scale properties of asteroids. Therefore we use the lifting scheme [10]. It consists of adding to each vertex of the set $\{v^1\}$ a linear combination of the nearest wavelet details located at the midpoints (see Fig. 4 b). If the vertex v is surrounded by N coefficients w_i the approximation a at the same site is given by:

$$a = v + \frac{3}{4}\sum_{i=1}^{N} w_i \tag{3}$$

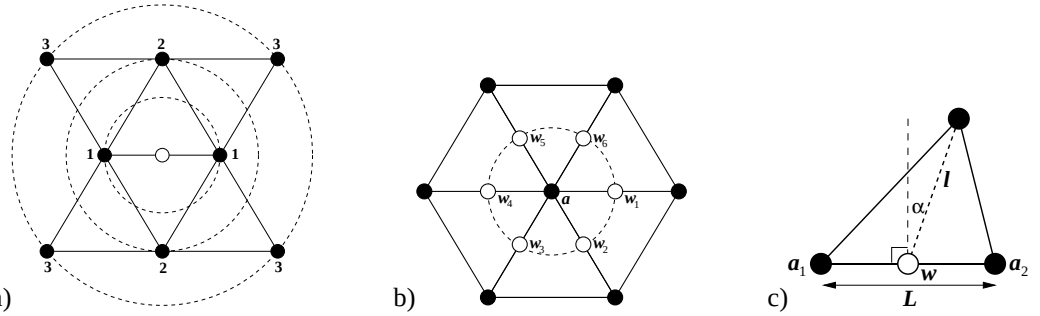

Figure 4: a) Prediction of a new vertex (white) from existing vertices (black) in the regular case, using 3 neighborhood orders as indicated by the numbers. b) Lifting scheme: wavelet coefficients w_i (white) around an approximation coefficient a (black). c) Wavelet coefficient normalization: lenghts L and l, angle α.

The transform is critically sampled, since the detail and approximation coefficients replace the original ones at each level. The maximum level is given by the depth of the subdivision J. It is simple to invert, starting with the lifting step and replacing the addition in Eq. (3) by a subtraction, then predicting the midpoints from using Eq. (1) and adding the wavelet coefficients w. So it is easy to see that the subdivision is an inverse wavelet transform with all detail coefficients set to zero, and one can then imagine a straightforward application: mesh smoothing (forward transform, shrinking detail coefficients and inverse transform) [4].

The tool presented here can perform the multiresolution analysis [3] of a surface for any topology. It is fast (linear complexity w.r.t. the number of vertices) and performs in-place computations.

2.4 Coefficient interpretation: local scale and direction

Now that we can decompose an asteroid surface model in a wavelet basis, we have to pay a particular attention to the meaning of the detail coefficients. The used decomposition scheme is semi-uniform [1] since it is done on a semi-regular grid. The uniformity is only topological. The wavelet functions are actually defined in this topological space and do not reflect the local geometry of the studied object (they do not depend on the local spacing between vertices). Thus, the wavelet coefficients encode absolute variations of the geometry between two approximation levels, regardless of the size of the triangles in the mesh. However, a given variation does not have the same meaning for different point densities: the higher the density, the bigger the feature related to this geometry variation. To account for that, we need to define the notion of local scale.

We have not used the word "scale" previously, we rather talk about "levels" of the transform, because we define the scale locally for each coefficient rather than globally for each level. Accordingly, when considering all the coefficients of a given level, there is a mixing of various scales depending on the local mesh density. We define the local scale as:

$$s = L\left(\frac{3}{4}\frac{L^2}{l^2}(\cos\alpha + \sin\alpha)^2 + 4\right)^{-1/2} \tag{4}$$

such that we can account for local deformation of each triangle (see Fig. 4 c). L is the length of the edge a_1a_2 in the approximation mesh, and l is a distance from w to a parent of order 2, α encoding the skew of the triangle. The scale for w is actually an average of the two scales computed for both triangles sharing the edge a_1a_2.

We claim that this is the right way to treat the problem of non-uniformity of the mesh, instead of trying to normalize the wavelet functions themselves (which does not make sense in our approach, since they are defined on the semi-regular topological support). Any detail coefficient w is supplemented with a local scale s which helps interpreting it or affecting a model to it.

Like the approximation coefficients, the wavelet details are 3D vectors. The former have an obvious meaning, i.e. the same object at different resolutions, whereas the latter embed details both along and orthogonal to the surface. To provide a really useful analysis tool, we have to separate these two components, thus enabling the user to perceive real geometric details (variations normal to the surface, denoted $w_\perp$) and not mixing them with the irregularities of the surface sampling (variations parallel to the surface $w_\parallel$). The local normal is determined with the same triangles as in the scale computation. Finally, the multiresolution decomposition at depth J consists of the set of J levels of details $w_\perp + w_\parallel$ associated with local scales s, and one coarse approximation a.

3 EXPERIMENTS: ASTEROID EROS

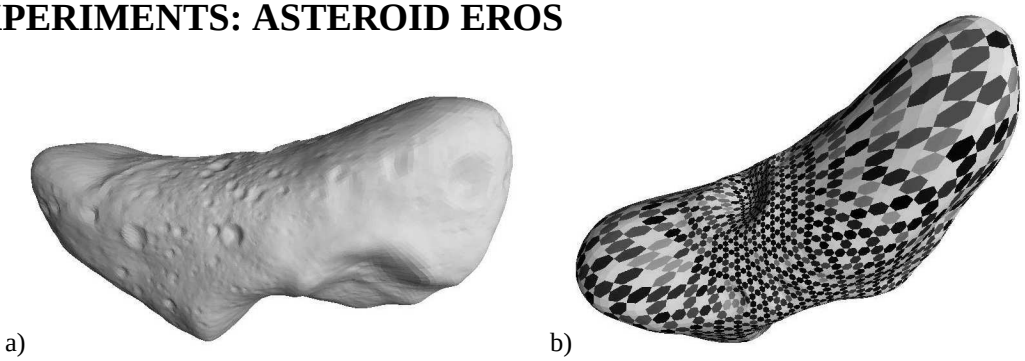

a) b)

Figure 5: a) Model of the asteroid 433 Eros, using a subdivided mesh (level 6, 40962 vertices), using the NEAR laser rangefinder data. b) Normal wavelet coefficients $w_\perp$ at level 2, shown on a subdivided version of the coarse approximation at level 2 (the vector norm is represented by different gray levels; minimum is black).

3.1 Example of wavelet transform of the asteroid

Fig. 5 shows a subdivided mesh model of Eros initialized with a spherical height field; the geometry is given by the NEAR laser rangefinder [13]. An illustration of the normal wavelet coefficients at level 2 is also shown. Fig. 6 shows approximations of the asteroid surface at different resolutions; all the details disappearing between two successive levels of approximation are encoded in the detail coefficients. In general, we have observed that the finest levels of details capture most of the small craters, while other levels capture larger ones, as well as ridges or valleys.

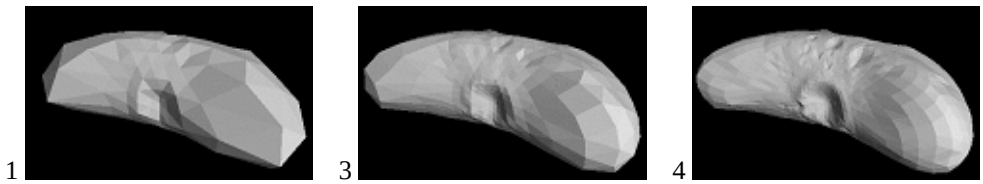

Figure 6: Multiresolution approximations of the model Fig. 5 at levels 2, 3 and 4.

3.2 Illustration of the scale invariance

Let us check whether the amplitude spectrum of the asteroid can be modeled by a scale invariant law. This spectrum is defined by the average size σ of the details (given here by the wavelet detail coefficients $w_\perp$) for each spatial frequency f (here we assume we can use the inverse of the scale, i.e. $s = 1/f$). The scale invariance implies $\sigma(r) = \sigma_0\, f^{-q}$, which describes the so-called "1/f" noise, a widely used model for natural objects [6, 9].

The model displays the good agreement between this model and the data (Fig. 7); we have represented as a log-log plot the average amplitude of the detail coefficients as a function of their local scale, and the plot is in accordance with the following equation:

$$\log E\left[|w_{i\,\perp}|\right] \simeq q\, \log(s_i) + \log \sigma_0 \tag{5}$$

where the expectation is taken w.r.t. time and space as well. The parameter q, or fractal exponent, is related to the fractal dimension D by $D = T + (3/2 - q)$ where T is the topological dimension of the surface, i.e. $T \equiv 2$. We get $D \simeq 2.38$ for the surface of Eros.

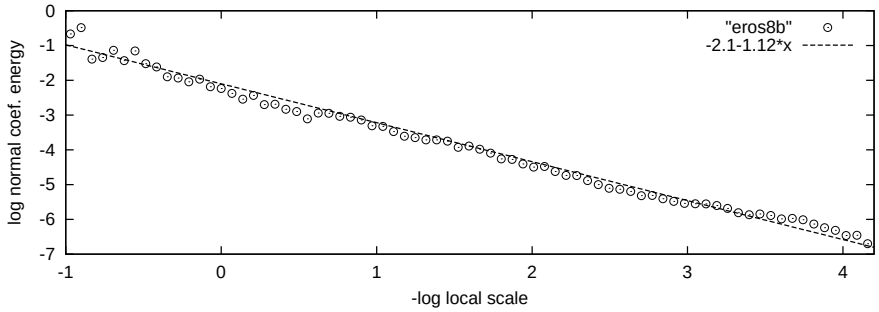

Figure 7: Log-log plot representing the size of the wavelet details of the asteroid Eros as a function of the local scale, illustrating the statistically scale-invariant behaviour of the surface.

4 A MULTISCALE MODEL FOR FRACTAL SURFACES

The spectrum model presented above can be seen as a probabilistic model of the wavelet coefficients. It is closely related to a fractional Brownian motion [11], used to describe natural images. We propose to extend this kind of model to natural surfaces, assuming that each normal wavelet detail coefficient is an independent random variable following a zero-mean Gaussian distribution. Eq. (5) leads to:

$$P\left(\{w_\perp\}\right) \propto \prod_i \exp\left(-\lambda_i\ (s_i)^{-2q}\ |w_{i\,\perp}|^2\right) \tag{6}$$

where λ_i are smoothness parameters depending on the spatial position only. Thus, we construct a spatially adaptive fractal model applicable to a broad range of natural surfaces, whose properties are generally spatially varying. On the other hand, the parallel coefficients $w_\parallel$ are related to the smoothness of the sampling and their value should not have any influence on the object shape. A model involving them could be used as a sampling regularity prior, whereas the model of Eq. (6) acts as a surface smoothness prior.

5 APPLICATIONS

3D object reconstruction from multiple images
One of the most powerful applications of smoothness priors is in ill-posed inverse problems, because of their regularizing properties; they act as stabilizers and constraints on the solution, taking great advantage of the available prior knowledge. A challenging problem is 3D surface reconstruction from several corrupted observations (noisy 2D images) [5]. Within a Bayesian framework, a likelihood function (related to the image formation process) and the prior model are combined to form a posterior density, which is maximized w.r.t. the geometry and all the model parameters to perform the surface reconstruction. Using the new fractal model should enable us to dramatically enhance the result quality and the computation speed and stability, thanks to the multiscale approach.

Fractal geometry and synthetic images
The proposed model can also be used to generate synthetic asteroids or planetary surfaces, and to simulate realistic reflectance functions [9] based on the physically-consistent fractal assumption rather than empirical models.

6 CONCLUSION

In this paper, we have shown how to build a linear and critically sampled wavelet transform on meshes of arbitrary topology; our contributions consist of combining one of the smoothest subdivision schemes with lifted wavelets, and complementing the wavelet coefficients with a local scale estimate. We have illustrated the fractal nature of asteroids by checking the statistical self-similarity of 433 Eros, using the proposed transform. Thus, we have derived a new model for natural surfaces, applicable to 3D object reconstruction or synthesis.

As an analysis tool, the proposed normal/parallel coefficient decomposition performs well on highly irregular shapes such as asteroids, enabling one to distinguish between shape details and sampling irregularity. However, for a spherical object such as a planet, whose natural features are small compared to its radius, the normal coefficients are corrupted by the geometry of the sphere, even though we expect them to only capture the details – i.e. deviations from a smooth surface. Indeed, the decomposition of a sphere does not provide null coefficients (whereas the decomposition of a planar surface does). We could extend the current approach by considering the support of the data to be the irregular geometric mesh instead of the semi-regular topological support of the present study. A scalar potential would then be affected to each vertex, e.g. the altitude in the case of a planet.

This work was done while in the Bayes team led by Peter Cheeseman (part of the Computational Sciences Division at NASA Ames), and partially supported by an INRIA Postdoc grant in 2002.

References

[1] I. Daubechies and W. Sweldens. Wavelets on irregular pointsets, 1999.

[2] N. Dyn, J. Gregory, and D. Levin. A butterfly subdivision scheme for surface interpolation with tension control. *ACM Trans. Graph.*, 9:160–169, 1990.

[3] M. Eck, T. DeRose, T. Duchamp, H. Hoppe, M. Lounsbery, and W. Stuetzle. Multiresolution analysis of arbitrary meshes. *Computer Graphics*, 29(Annual Conference Series):173–182, 1995.

[4] I. Guskov, W. Sweldens, and P. Schröder. Multiresolution signal processing for meshes. In Alyn Rockwood, editor, *Siggraph 1999, Computer Graphics Proceedings*, pages 325–334, Los Angeles, 1999. Addison Wesley Longman.

[5] R.D. Morris, P. Cheeseman, V.N. Smelyanskiy, and D.A. Maluf. A bayesian approach to high resolution 3D surface reconstruction from multiple images. *Proc. of the IEEE Workshop on Higher Order Statistics*, 1999.

[6] A. P. Pentland. Fractal-based description of natural scenes. *IEEE Trans. Pattern Anal. Machine Intell.*, 6:661–675, 1984.

[7] P. Schröder. Subdivision for modeling and animation, 1998.

[8] P. Schröder and W. Sweldens. Spherical wavelets: efficiently representing functions on the sphere. *Computer Graphics*, 29(Annual Conference Series):161–172, 1995.

[9] K. Seidel and M. Datcu. Fusion of real and synthetic images for remote sensing scene understanding. *FRACTAL'93, Kingston, UK*, 1993.

[10] W. Sweldens. The lifting scheme: A construction of second generation wavelets. *SIAM Journal on Mathematical Analysis*, 29(2):511–546, 1998.

[11] G. Wornell. *Signal processing with fractals: a wavelet-based approach*. Signal processing series. Prentice Hall, 1995.

[12] D. Zorin, P. Schröder, and W. Sweldens. Interpolating subdivision for meshes with arbitrary topology. *Computer Graphics*, 30(Annual Conference Series):189–192, 1996.

[13] M.T. Zuber, D.E. Smith, A.F. Cheng, J.B. Garvin, O. Aharonson, T.D. Cole, P.J. Dunn, Y. Guo, F.G. Lemoine, G.A. Neumann, D.D. Rowlands, , and M.H. Torrence. The shape of 433 Eros from the NEAR-Shoemaker laser rangefinder. *Science*, pages 2097–2100, 2000.